Nanoscale

PAPER

View Article Online
View Journal

Cite this: DOI: 10.1039/d3nr05810g

Surface plasmon enhancement in silver nanowires and bilayer two-dimensional materials†

Weibin Zhang, [a] Cunwei Kong,[a] Xinfeng Zhang,[a,b] Quan Wang *[a,c] and Wei Xue*[d]

Received 15th November 2023,
Accepted 30th January 2024

DOI: 10.1039/d3nr05810g

rsc.li/nanoscale

In order to improve the low light absorption of two-dimensional (2D) transition metal dichalcogenides (TMDCs), surface plasmon (SP) nanostructures have been widely studied. However, the impact of interlayer twist on such nanostructures has rarely been studied. Here, we construct two different composite structures of silver nanowires (Ag NWs) and pristine bilayer MoS_2 (pBLM) or twisted bilayer MoS_2 (tBLM). The interlayer twist can further promote the light utilization of MoS_2, resulting in an ~4-fold higher spectral enhancement in Ag/tBLM than that in Ag/pBLM. In addition, the photocurrent and detectivity of the phototransistor based on the Ag/tBLM composite structure were improved by 7-fold and ~100-fold, respectively, compared to those of the Ag/pBLM phototransistor. Theoretical simulations show that the enhancement of photocurrent can be attributed to the enhancement of the local electric field at the interface between Ag NWs and the tBLM film, which is called the 'hot spot'. These results provide a reference for understanding the modulation mechanism of SPs and interlayer twist on the optoelectronic properties of 2D materials.

1. Introduction

In the past few years, the research on new two-dimensional (2D) material optoelectronic devices has been developing rapidly.[1–3] MoS_2 is a typical transition metal dichalcogenide with remarkable physical and chemical properties. However, its single atomic layer thickness limits the light absorption of MoS_2, which hinders its application in the field of optoelectronic devices.[4,5]

Combining MoS_2 with plasmonic nanostructures provides a solution to enhance the absorption of 2D semiconductor materials.[6–8] In recent years, materials such as nanowires (NWs),[9,10] nanospheres,[11,12] nanodisks,[13,14] nanorods[15] and nanocubes[16] have been tried to combine with MoS_2 to improve its light absorption. Resonant noble metal nanostructures can generate localized surface plasmon resonance, which can strongly limit the light field and therefore increase the luminous energy intensity of 2D materials.[17,18] Localized surface plasmon (LSP) generates strong light confinement near metal nanostructures. The LSP effect can significantly enhance the optical absorption and emission of the upper and lower transition metal dichalcogenide (TMDC) layers of metal nanostructures.[19,20] Based on this mechanism, several structures for optimizing the enhancement effect have been proposed. For instance, Ji *et al.*[21] achieved a four-fold photocurrent enhancement by integrating Au–SiO_2 core–shell nanoparticles into the channel of MoS_2 phototransistors using localized surface plasmon. Although this method is convenient, the photocurrent increase is not high. Li *et al.*[22] presented an Au nanoparticle grating structure, which can more than double the light absorption under 532 nm illumination. However, this process is complex and has high requirements for accuracy and temperature. In addition, Wu *et al.* found that the Ag nanoparticle/Au film cavity structure generates a gap plasma mode, which makes the photocurrent extracted from the MoS_2 film placed in the plasmonic cavity increase tremendously.[23] Nevertheless, these plasma structures usually require multiple complex manufacturing steps, which are not only expensive, but also time-consuming.[24,25] Hence, it would be advantageous to be able to design plasmonic structures that can be realized through simple processing steps and exhibit obvious performance enhancement.

Interlayer twist provides a new degree of freedom for 2D material modification.[26–28] By adjusting the twist angle, the indirect band gap of bilayer MoS_2 can be extended from 1.38 eV to 1.54 eV.[26] In addition, the interlayer twist can effectively

[a]Zhenjiang Key Laboratory of Advanced Sensing Materials and Devices, School of Mechanical Engineering, Jiangsu University, Zhenjiang 212013, China. E-mail: wangq@ujs.edu.cn
[b]Jiangsu Zorrun Semiconductor Co., Ltd, Nantong 226500, China
[c]State Key Laboratory of Transducer Technology, Chinese Academy of Sciences, Shanghai 200050, China
[d]Oujiang Laboratory (Zhejiang Lab for Regenerative Medicine, Vision and Brain Health), Wenzhou, Zhejiang, P.R. China. E-mail: xw@wzu.edu.cn

†Electronic supplementary information (ESI) available. See DOI: https://doi.org/10.1039/d3nr05810g

adjust the coupling strength of bilayer TMDCs, thus affecting the Raman characteristics and PL indirect exciton energy of the semiconductor TMD moiré nano superlattice.[29,30] Here, we propose a composite structure that combines MoS_2 interlayer twist with Ag NW surface plasmons. By comparing the spectral gain effect of Ag NWs on twisted bilayer MoS_2 (tBLM) and pristine bilayer MoS_2 (pBLM) films, the impact of interlayer twist on the coupling of Ag NW surface plasmon polaritons with MoS_2 excitons was studied. It is found that interlayer twist can effectively enhance the light absorption of MoS_2 and improve the optoelectronic properties of Ag/MoS_2 phototransistors.

2. Experimental

As shown in Fig. S1a,† Ag/tBLM phototransistors were fabricated on a SiO_2 (285 nm) substrate with p + –Si as the back gate electrode. The source and drain contacts are made of Au/Cr metal stacks with thicknesses of 50 and 5 nm, respectively.

Monolayer MoS_2 films were prepared by mechanical exfoliation. A large-size film (>15 μm) with flat and smooth edges was selected and divided into two by the tip of the probe. One film was transferred to the electrode and then the other film was transferred to the former at a certain twist angle to complete the preparation of the tBLM sample (as shown in Fig. S1b†).

Besides, large-sized silver nanowires (200 nm in average diameter) were prepared by a multi-step polyol reduction method with $FeCl_3$ as the control agent, ethylene glycol as the reducing agent, $AgNO_3$ as the precursor and PVP as the adsorbent. The SEM and STM images of Ag NWs are shown in Fig. S2.† Finally, the Ag NWs were integrated into the tBLM film with a fiber taper to complete the device fabrication (as shown in Fig. S1c†).

Raman and PL spectra were recorded using a laser with a wavelength of 520 nm on a microspectral scanning test system (Metatest, MStarter 100). The laser power on the sample was about 0.5 mW to prevent the overheating effect. In our experiment, the diameter of the spot is 20 μm at focus. The same sampling time was selected for all spectral scanning processes. All measurements were carried out at room temperature and under normal conditions.

The electronic characteristics of the phototransistors were tested on a high-precision photocurrent scanning test system (Metatest, MStarter 200). In the photoelectric measurement, the relevant laser beam was irradiated onto the surface of the substrate by clamping the optical fiber with iron brackets. Excitation light with a wavelength of 520 nm was selected and the laser power density was set to 10^5 mW cm^{-2}. All measurements were performed at room temperature and in a normal environment.

In order to explore the mechanism of spectral enhancement in Ag NW and tBLM composite structures, the 2D frequency domain method was used to simulate the surface local electric field of the Ag NW and Ag/tBLM composite structure on the SiO_2 substrate. In the simulation model, the light source is the full-field scattering field light source. The wavelength of excitation light was set to 520 nm and propagated along the *z*-axis. Besides, 12 perfectly matched layers were used along the *z*-axis to avoid reflections. The size of the simulation area was set to 4 μm × 4 μm and the grid accuracy was set to 0.2 nm to obtain accurate results of the field distribution in the composite structure. The dielectric constants of MoS_2, SiO_2 and Ag NWs were obtained from the study of Palik *et al.*[31] and Hsu *et al.*[32] The thickness of the tBLM layer was set to 1.3 nm, and the radius and length of Ag NWs were 100 nm and 1 μm, respectively. The monitor was placed perpendicular to the *y*-axis to get a side view of field distribution.

The device structure is shown in Fig. 1a. Fig. 1b and S3† show the optical microscopy images of the Ag/MoS_2 devices. According to Debnath *et al.*[33] and Zhang *et al.*,[34] the upper and lower layers of tBLM and twist angles are marked in Fig. 1b. The optical absorption characteristics of MoS_2 were determined by exciton transitions. Two characteristic peaks located in the red to near-infrared band are usually called the A peak (1.83 eV) and the B peak (1.98 eV). They are all related to the optical transition from the highest spin splitting valence band to the lowest conduction band.[35] As shown in Fig. 1c, the PL intensity of the Ag/tBLM composite region is significantly higher than that of tBLM, and the spectrum is not distorted. Similarly, the PL spectral enhancement was also found in pBLM, as shown in Fig. S4.† The causes of this phenomenon will be shown later. The interlayer twist affects this gain effect, and the enhancement factor is 4.

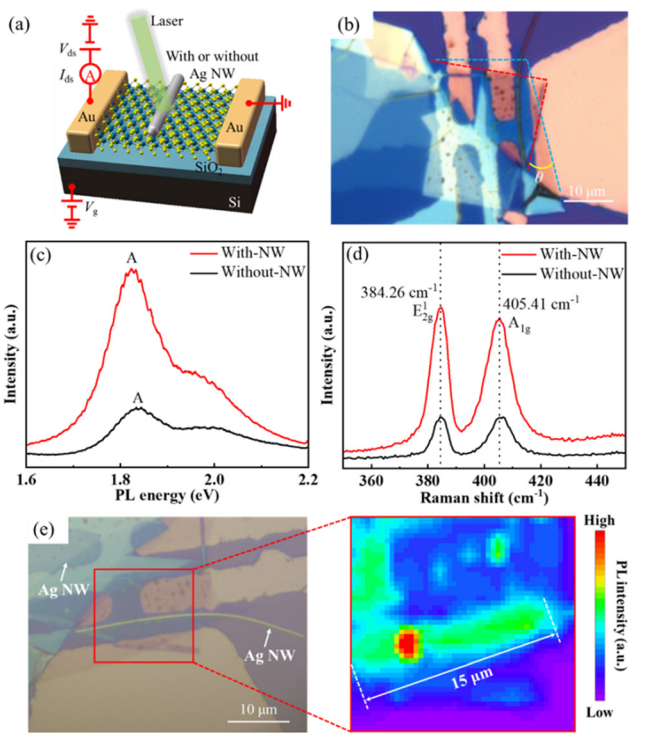

Fig. 1 (a) Device structure and (b) optical microscopy diagram of the Ag/tBLM device. (c) PL and (d) Raman spectra of the Ag/tBLM composite structure. (e) PL intensity mapping of the device.

3. Results and discussion

3.1 Spectral characterization of the devices

The Raman spectrum test results is shown in Fig. 1d and the number of layers can be judged by the peak spacing between the E_{2g}^1 peak and the A_{1g} peak.[36,37] When the peak spacing is less than 20 cm^{-1}, it can be judged as a single-layer film. When the peak spacing is 20–22 cm^{-1}, it can be judged as a double-layer film. The Raman peak spacing of this sample is 21.15 cm^{-1}, so it is determined to be a double-layer film. It can be clearly seen that under the action of Ag NW surface plasmon, the Raman intensity of the composite region of tBLM is enhanced, and the maximum is also increased by nearly 4 times (compared with Fig. S5†). In the Ag/tBLM composite structure, the SPs of Ag NWs make the light field bound and enhanced, thus improving the Raman and PL intensities of tBLM. At the same time, the E_{2g}^1 peak and the A_{1g} peak of the composite region did not shift significantly compared with the peak of pure tBLM, indicating that the stress and doping have little effect on the material, which is consistent with the results obtained by PL spectrum analysis.

According to the PL and Raman spectral test results, the PL intensity mapping test was performed on Ag/pBLM and Ag/tBLM composite structures. As shown in Fig. S6,† limited by the line contact between Ag NWs and the channel material, only the PL intensity in the middle region of the Ag/pBLM composite structure is significantly enhanced, indicating that the surface plasmon is localized. Although this LSP can produce a strong local field enhancement effect, the PL intensity of the Ag NW region except for the center is 60% lower. The size and location of the enhancement region are affected by the contact area between Ag NWs and tBLM films and the relative position of Ag NWs, tBLM and Au electrodes, respectively.[9,21] The Au electrodes absorb and shield part of the PL of tBLM, resulting in poor quality of the PL spectrum. Therefore, the maximum enhancement location appears in the tBLM region near the Ag NWs and away from the Au electrodes. Interestingly, we found that this LSP was improved under the effect of interlayer twist. As shown in Fig. 1e, the PL intensity is enhanced by 5 times and 3 times in the circular region of the Ag/tBLM composite structure and the long strip region along the Ag NWs, respectively. As shown in the illustration in Fig. 1e, the extra spectral enhancement distance is about 15 μm. We believe that the interlayer twist not only affects the interlayer coupling of MoS_2, but also changes the coupling strength between the excitons of MoS_2 and the SPs of Ag NWs.

3.2 Simulation analysis of the composite structure

We established a three-dimensional simulation model as shown in the illustration of Fig. 2a and b to explain this spectral enhancement phenomenon. It is found that the maximum electric field strength at the interface between the SiO_2 substrate and Ag NWs is weak. When Ag NWs are placed on tBLM, the electric field exhibits a 'hot spot' effect, and the maximum electric field strength is obviously enhanced. This phenomenon is also reflected in the electric field strength curve. The

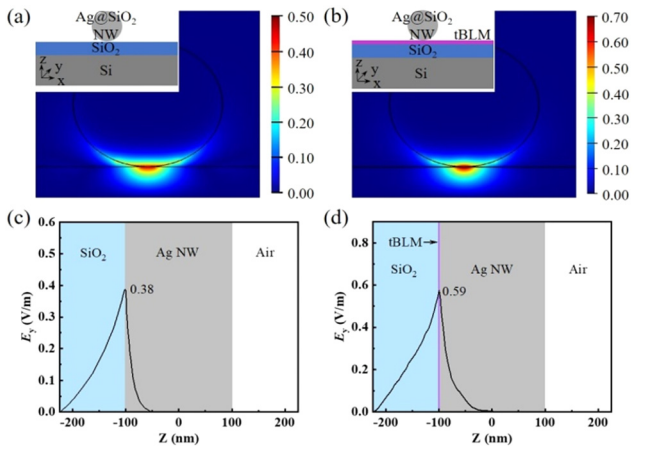

Fig. 2 (a) Electric field distribution and (c) intensity diagrams of Ag NWs on the SiO_2 substrate. (b) Electric field distribution and (d) intensity diagrams of Ag/tBLM on the SiO_2 substrate. Inset: cross section of the simulation model.

introduction of tBLM can enhance the maximum electric field intensity and make the electric field more localized. The strong LSP from the 'hot spot' drastically improved the light–matter interaction of tBLM and thus significantly enhanced the PL intensity.[9] In addition, the integral of the electric field strength in both cases was calculated, as shown in Fig. 2c and d. It is found that the electric field intensity integral on Ag/tBLM is 55.3% higher than that on Ag NWs. The simulation results are consistent with the experimental results. Under a 520 nm laser, the SPs in the Ag NWs were excited and coupled with MoS_2, which plays a spectral enhancement role.

3.3 Electrical test of the devices

In order to further study the photoelectric properties of this composite structure, we first tested the output characteristic curves, as shown in Fig. 3a, b and S7.† The linearity and symmetry of the curve indicate that a good ohmic contact is formed between the electrode and the channel material. The slope of the curve increases with the increase of gate voltage, indicating that the gate voltage has a good modulation effect on the carrier concentration in the channel. The source–drain current I_{ds} of the device is significantly improved under the light field, indicating that the device has good light sensitive characteristics.

According to the following formulas, the photoresponsivity (R) and the specific detectivity (D^*) of the Ag/MoS_2 phototransistors can be calculated.

$$R = \frac{I_{\text{illumination}} - I_{\text{dark}}}{P} \quad (1)$$

$$D^* = \frac{R\sqrt{A}}{\sqrt{2eI_{\text{dark}}}}. \quad (2)$$

Here, P is the incident laser power and A is the area of the channel.

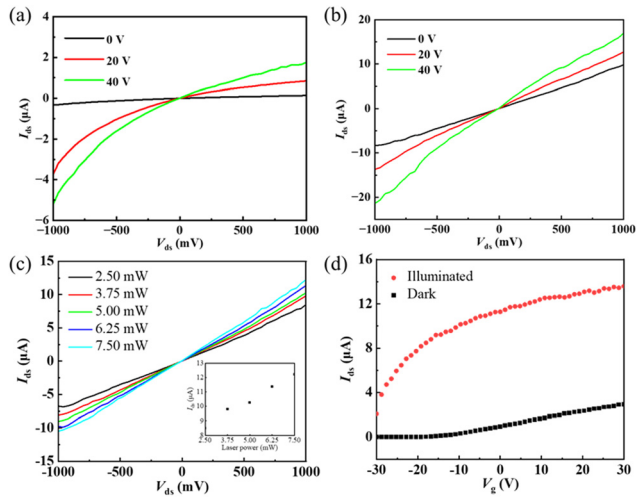

Fig. 3 Output characteristic curves of the Ag/tBLM device: (a) without light and (b) under irradiation with a 520 nm laser. (c) Output characteristic curve of the device under irradiation with a laser of different powers. (d) Transfer characteristic curve of the Ag/tBLM device.

The photoresponsivity of the Ag/pBLM phototransistor is 2.64 mA W^{-1}, which is about 4 times higher than that of the device without Ag NWs (as shown in Fig. S8†). The Ag/tBLM phototransistor has a photoresponsivity of 25.04 mA W^{-1}, which is one order of magnitude higher than the Ag/pBLM device. The specific detectivity of the Ag/tBLM phototransistor is 7.30×10^8 Jones, which is two orders of magnitude higher than that of the Ag/pBLM device, and is 40 times higher than the tBLM device without Ag NWs. The photocurrent and responsivity of the Ag/tBLM device are higher than those of some previously reported devices,[21,27,38,39] as shown in Table 1. The incident photon energy activates the defect-based trap states, which act as recombination centers, thus helping to improve the detection performance.[38] However, the existence of traps/defects in MoS_2 may be the reason for the slow photoresponse speed of the device.

Table 1 Comparison of the Ag/tBLM device fabricated in this work with the previously reported MoS_2 devices

Photocurrent (μA)	Responsivity (mA W^{-1})	Detectivity (Jones)	Ref.
0.08	0.56	3.13×10^4	21
3	13.05	1.83×10^7	27
10	13.15	1.11×10^{11}	38
0.04	1.10	3.86×10^{10}	39
14.74	25.04	7.30×10^8	This work

In addition, the photoelectric response of the device at different optical powers was also tested. It can be seen from Fig. 3c that the increase of source–drain voltage accelerates the drift rate of carriers, which shortens the drift time of carriers in the channel. At the same time, the increase of laser power leads to an increase in the number of incident photons, resulting in more photogenerated carriers in the channel material. The slope of the curve in the figure also changed significantly. However, as the laser power further increases, the absorption of the channel material to light gradually approaches saturation. The recombination probability of electrons and holes gradually increases, resulting in a slowdown in the increase of photocurrent, which is reflected in the gradual decrease in the increase of the slope of the curve.

Fig. 3d shows the transfer characteristic curve of the Ag/tBLM phototransistors. The source–drain current increases with the increase of gate voltage, reflecting that the transistor is n-channel type and the carrier is electrons. Under a negative gate voltage, the difference between the photocurrent and the dark current decreases with the decrease of gate voltage. The transfer characteristic curve demonstrates that the signal-to-noise ratio of the device is improved under gate voltage regulation. According to Fig. S9,† the photocurrent of the Ag/pBLM phototransistor is 2.15 μA. When subject to the atomic layer absorption of MoS_2, the photocurrent of the pBLM phototransistor without Ag NWs is small under 520 nm laser irradiation. When the back gate voltage is 30 V, the photocurrent is 0.25 μA, which is one order of magnitude lower than that of the Ag/pBLM phototransistor. The photocurrent of the Ag/tBLM phototransistor is 14.74 μA, which is about 7 times

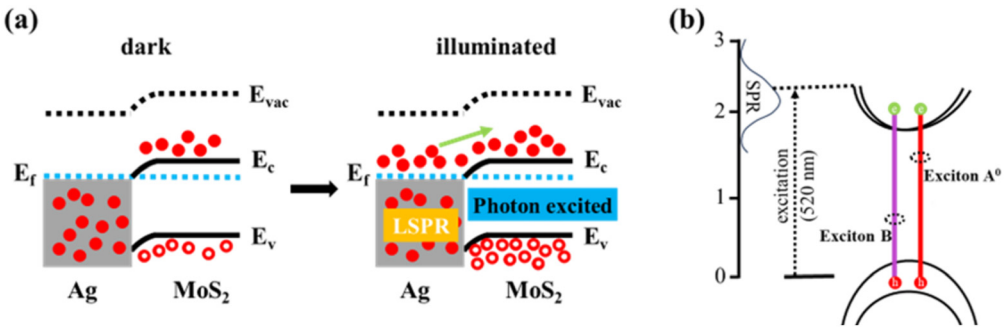

Fig. 4 (a) Energy band diagram of LSPR-enhanced MoS_2 phototransistor performance. E_c, E_v and E_{vac} represent the conduction band minimum (CBM), the valence band maximum (VBM) and the vacuum level, respectively.(b) Schematic diagram of the plasmon coupling mechanism of the Ag/MoS_2 composite structure.

higher than that of the Ag/pBLM one. The interlayer twist changes the relative position and spacing between the upper and lower layers of S and Mo atoms and changes the interlayer coupling strength. The coupling strength between the SPs of Ag NWs and the excitons of MoS_2 is further affected. This results in photoelectric performance gain effects of Ag NWs on MoS_2 phototransistors with interlayer twist.

3.4 Mechanism analysis

The mechanism of the enhanced photoluminescence and photocurrent of MoS_2 and the surface plasmon coupling of Ag NWs is shown in Fig. 4. The improved photocurrent of MoS_2 photodetectors modified with Ag NWs could be attributed to the enhancement of local electric field caused by the local surface plasma resonance (LSPR) effect. Therefore, we describe the energy band diagram of the Ag/MoS_2 composite structure shown in Fig. 4a to illustrate the carrier injection process. Due to Ag has a lower work function than MoS_2 (Ag: ~4.26 eV and MoS_2: ~5.20 eV), when they come into contact, the energy band of MoS_2 will bend downwards to achieve Fermi level equilibrium.[40,41] When irradiated with incident light, many oscillating electrons appear on the surface of Ag NWs. Then, as the electrons of Ag NWs continue to transfer to MoS_2, the carrier density of MoS_2 increases. Upon excitation with a 520 nm laser, which is close to the SPR wavelength of Ag, a plasmonic hot spot is formed at the junction of Ag NWs and MoS_2, and hence serves as a source of LSPR, as shown in Fig. 4b. In addition, there is a coupling between the excitons of MoS_2 and the SPs of Ag NWs, resulting in an enhanced excitation and PL intensity.

4. Conclusions

In summary, based on the optical and electrical performance tests of the phototransistors with Ag/MoS_2 composite structures, we explored the coupling mechanism between the excitons of MoS_2 and the SPs of Ag NWs. Through the frequency domain simulation, it was found that the introduction of tBLM can increase the electric field intensity integral on Ag NWs by 1.55 times and make the electric field more localized. A significant intensity enhancement of the PL and Raman spectra has been achieved in the Ag/MoS_2 composite structure with interlayer twist. The photoresponsivity and detectivity of the Ag/tBLM phototransistor are ~10-fold and ~100-fold higher than those of the Ag/pBLM one, respectively. This work has made a useful exploration for improving the interaction between light and matter in MoS_2 and provides a reference for structural design to improve the optoelectronic performance of 2D semiconductor devices.

Author contributions

W. Zhang: writing – original draft and investigation. C. Kong: investigation. X. Zhang: formal analysis. Q. Wang: review and editing, supervision, and funding acquisition. W. Xue: supervision.

Conflicts of interest

There are no conflicts to declare.

Acknowledgements

The authors acknowledge the support from the Jiangsu Agriculture Science and Technology Innovation Fund (No. CX (21)1007).

References

1 A. J. Yang, S. X. Wang, J. W. Xu, X. J. Loh, Q. Zhu and X. R. Wang, *ACS Nano*, 2023, **17**, 9748–9762.
2 L. Q. Zhuo, D. Q. Li, W. D. Chen, Y. Zhang, W. Zhang, Z. Q. Lin, H. D. Zheng, W. G. Zhu, Y. C. Zhong, J. Y. Tang, G. G. Lu, W. X. Fang, J. H. Yu and Z. Chen, *Nanophotonics*, 2022, **11**, 1137–1147.
3 M. D. Du, X. Q. Cui, B. Zhang and Z. P. Sun, *ACS Photonics*, 2022, **9**, 2825–2832.
4 M. Bernardi, M. Palummo and J. C. Grossman, *Nano Lett.*, 2013, **13**, 3664–3670.
5 H. S. Tsai, Y. H. Huang, P. C. Tsai, Y. J. Chen, H. Y. Ahn, S. Y. Lin and Y. J. Lu, *ACS Omega*, 2020, **5**, 10725–10730.
6 G. F. Yang, X. D. Fang, Y. Gu, N. Y. Lu, X. M. Zhang, Y. K. Wang, B. Hua, X. F. Ni, Q. Fan and X. Gu, *Appl. Surf. Sci.*, 2020, **508**, 144794.
7 H. T. Chen, J. Yang, E. Rusak, J. Straubel, R. Guo, Y. W. Myint, J. J. Pei, M. Decker, I. Staude, C. Rockstuhl, Y. R. Lu, Y. S. Kivshar and D. Neshev, *Sci. Rep.*, 2016, **6**, 22296.
8 L. Lu, T. T. Zhao, L. Chen, C. Y. Wang, Z. Q. Zhou and X. F. Ren, *Nanotechnology*, 2022, **33**, 155401.
9 S. Bang, N. T. Duong, J. Lee, Y. H. Cho, H. M. Oh, H. Kim, S. J. Yun, C. Park, M. K. Kwon, J. Y. Kim, J. Kim and M. S. Jeong, *Nano Lett.*, 2018, **18**, 2316–2323.
10 H. S. Lee, M. S. Kim, Y. Jin, G. H. Han, Y. H. Lee and J. Kim, *Adv. Opt. Mater.*, 2015, **3**, 943–947.
11 D. H. Luong, H. S. Lee, G. Ghimire, J. Lee, H. Kim, S. J. Yun, G. H. An and Y. H. Lee, *Small*, 2018, **14**, 1802949.
12 A. Sobhani, A. Lauchner, S. Najmaei, C. Ayala-Orozco, F. F. Wen, J. Lou and N. J. Halas, *Appl. Phys. Lett.*, 2014, **104**, 031112.
13 H. Y. Lan, Y. H. Hsieh, Z. Y. Chiao, D. Jariwala, M. H. Shih, T. J. Yen, O. Hess and Y. J. Lu, *Nano Lett.*, 2021, **21**, 3083–3091.
14 S. Butun, S. Tongay and K. Aydin, *Nano Lett.*, 2015, **15**, 2700–2704.
15 K. C. J. Lee, Y. H. Chen, H. Y. Lin, C. C. Cheng, P. Y. Chen, T. Y. Wu, M. H. Shih, K. H. Wei, L. J. Li and C. W. Chang, *Sci. Rep.*, 2015, **5**, 16374.

16 B. Sun, Z. Y. Wang, Z. Y. Liu, X. H. Tan, X. Y. Liu, T. L. Shi, J. X. Zhou and G. L. Liao, *Adv. Funct. Mater.*, 2019, **29**, 1900541.
17 S. M. Bahauddin, H. Robatjazi and I. Thomann, *ACS Photonics*, 2016, **3**, 853–862.
18 G. C. Wang, L. Li, W. H. Fan, R. Y. Wang, S. S. Zhou, J. T. Lue, L. Gan and T. Y. Zhai, *Adv. Funct. Mater.*, 2018, **28**, 1800339.
19 S. Najmaei, A. Mlayah, A. Arbouet, C. Girard, J. Léotin and J. Lou, *ACS Photonics*, 2014, **8**, 12682–12689.
20 J. Yan, C. Ma, P. Liu and G. Yang, *ACS Photonics*, 2017, **4**, 1092–1100.
21 C. M. Ji, H. Jia, C. Zhou, Q. Wang and W. Xue, *Phys. Chem. Chem. Phys.*, 2022, **24**, 8296–8302.
22 J. L. Li, C. B. Nie, F. Y. Sun, L. L. Tang, Z. J. Zhang, J. D. Zhang, Y. Zhao, J. Shen, S. L. Feng, H. F. Shi and X. Z. Wei, *ACS Appl. Mater. Interfaces*, 2020, **12**, 8429–8436.
23 Z. Q. Wu, J. L. Yang, N. K. Manjunath, Y. J. Zhang, S. R. Feng, Y. H. Lu, J. H. Wu, W. W. Zhao, C. Y. Qiu, J. F. Li and S. S. Lin, *Adv. Mater.*, 2018, **30**, 1706527.
24 Y. Li, J. G. DiStefano, A. A. Murthy, J. D. Cain, E. D. Hanson, Q. Q. Li, F. C. Castro, X. Q. Chen and V. P. Dravid, *ACS Nano*, 2017, **11**, 10321–10329.
25 S. Namgung, D. A. Mohr, D. Yoo, P. Bharadwaj, S. J. Koester and S. H. Oh, *ACS Nano*, 2018, **12**, 2780–2788.
26 W. F. Zhang, H. Hao, Y. J. Lee, Y. Zhao, L. M. Tong, K. Kim and N. Liu, *Adv. Funct. Mater.*, 2022, **32**, 2111529.
27 W. B. Zhang, F. H. Cheng, J. W. Huang and Q. Wang, *Phys. Status Solidi RRL*, 2022, **16**, 2200235.
28 B. H. Lin, Y. C. Chao, I. T. Hsieh, C. P. Chuu, C. J. Lee, F. H. Chu, L. S. Lu, W. T. Hsu, C. W. Pao, C. K. Shih, J. J. Su and W. H. Chang, *Nano Lett.*, 2023, **23**, 13061312.
29 S. X. Huang, L. B. Liang, X. Ling, A. A. Puretzky, D. B. Geohegan, B. G. Sumpter, J. Kong, V. Meunier and M. S. Dresselhaus, *Nano Lett.*, 2016, **16**, 1435–1444.
30 M. Z. Liao, Z. Wei, L. J. Du, Q. Q. Wang, J. Tang, H. Yu, F. F. Wu, J. J. Zhao, X. Z. Xu, B. Han, K. H. Liu, P. Gao, T. Polcar, Z. P. Sun, D. X. Shi, R. Yang and G. Y. Zhang, *Nat. Commun.*, 2020, **11**, 2153.
31 E. Palik, *Handbook of optical constants of solids Vol. 3*, Academic Press, San Diego, CA, USA, 1998.
32 C. W. Hsu, R. Frisenda, R. Schmidt, A. Arora, S. M. de Vasconcellos, R. Bratschitsch, H. S. J. van der Zant and A. Castellanos-Gomez, *Opt. Mater.*, 2019, **7**, 1900239.
33 R. Debnath, I. Maity, R. Biswas, V. Raghunathan, M. Jain and A. Ghosh, *Nanoscale*, 2020, **12**, 17272–17280.
34 W. B. Zhang, F. H. Cheng, J. W. Huang, H. T. Yuan and Q. Wang, *Phys. Lett. A*, 2021, **418**, 127709.
35 K. F. Mak, K. L. He, C. Lee, G. H. Lee, J. Hone, T. F. Heinz and J. Shan, *Nat. Mater.*, 2013, **12**, 207–211.
36 G. Plechinger, S. Heydrich, J. Eroms, D. Weiss, C. Schuller and T. Korn, *Appl. Phys. Lett.*, 2012, **101**, 101906.
37 Q. K. Qian, Z. F. Zhang and K. J. Chen, *Phys. Rev. B*, 2018, **97**, 165409.
38 R. Singh, C. Patel, P. Kumar, M. Dubey, S. Sriram and S. Mukherjee, *ACS Appl. Electron. Mater.*, 2022, **4**, 5739–5746.
39 M. Sharma, P. Aggarwal, A. Singh, S. Kaushik and R. Singh, *Nano Mater.*, 2022, **5**, 13637–13648.
40 S. H. Choi, Z. Shaolin and W. Yang, *J. Korean Phys. Soc.*, 2014, **64**, 1550–1555.
41 S. S. Chee, D. Seo, H. Kim, H. Jang, S. Lee, S. P. Moon, K. H. Lee, S. W. Kim, H. Choi and M. H. Ham, *Adv. Mater.*, 2019, **31**, 1804422.